SUPPORTING INFORMATION

Stabilization of Immobilized Enzymes via the Chaperone-like Activity of Mixed Lipid Bilayers

Andres F. Chaparro Sosa, Daniel F. Kienle, Rebecca M. Falatach, Jessica Flanagan, Joel L. Kaar[*]*, Daniel K. Schwartz*[*]

Department of Chemical and Biological Engineering, University of Colorado Boulder, Boulder, CO 80309

[*]*Corresponding Authors:*
Joel L. Kaar
University of Colorado Boulder
Department of Chemical and Biological Engineering
Campus Box 596
Boulder, CO 80309
Tel: (303) 492-6031
Fax: (303) 492-4341
Email: joel.kaar@colorado.edu

Daniel K. Schwartz
University of Colorado Boulder
Department of Chemical and Biological Engineering
Campus Box 596
Boulder, CO 80309
Tel: (303) 735-0240
Fax: (303) 492-4341
Email: daniel.schwartz@colorado.edu

Supporting Methods

Characterization of SLBs by FRAP

Vesicles containing 1% of DOPE-LR (Avanti Polar Lipids) were prepared and incubated prior to imaging as described previously. The incorporated DOPE-LR was photo-bleached by illuminating a circular area of radius ~20 μm with a 532 nm 50 mW Gaussian beam diode-pumped solid-state laser (Samba, Cobolt) for 3 s. During the recovery stage (i.e., post-bleaching), DOPE-LR was excited using an Intensilight C-HGFIE lamp (Nikon) with an excitation filter centered a 545 nm with a bandwidth of 30 nm (Semrock). Excitation and emission wavelengths were separated using a 575 nm dichroic mirror (Chroma). The fluorescent emission of DOPE-LR was further filtered with a 560 nm long pass filter (Semrock) and was captured with a Hamamatsu CMOS (ORCA-flash 4.0) camera at an acquisition time of 150 ms. Fluorescent recovery curves and mobile fractions were obtained using the ImageJ plug-in simFRAP.[1] Ensemble diffusion coefficients were determined by fitting the recovery curves to a two-dimensional diffusion model derived for lipid diffusion after photo-bleaching with a Gaussian laser beam.[2]

Data Filtering

To prevent image noise from being misidentified as objects, trajectories that were not trackable for 4 or more frames (including both excitations, totaling 240 – 280 ms) were discarded. Additionally, due to the unavoidable presence of protein aggregates and LB defects (e.g., discontinuities in the SLB), anomalous observations were removed from the results during post-process. Protein aggregates were identified as extremely bright objects, which could be attributed to the emission from more than one fluorophore within the same diffraction-limited

spot.[3] To exclude these extremely bright objects, median intensity distributions for each, donor and acceptor, channel were created and a three standard deviation threshold was established. Any trajectories that had a median intensity above the threshold were excluded. Defects in LBs usually lead to immobile or highly confined objects. Therefore, for lipid compositions forming continuous LBs upon vesicle fusion (containing ≤50% DOPG), trajectories with average diffusion coefficients <0.1 $\mu m^2\ s^{-1}$ were excluded from further analysis.[4]

Estimating Folding and Unfolding Rate Constants

For the studied system, bleaching of the acceptor dye occurs on a similar time scale as transitions in the folding state. As a result, the molecules that undergo a multiple transition prior to bleaching do not constitute a representative fraction of the population and thus cannot be used to estimate the folding and unfolding rates. Instead, the folding rates are determined by fitting the folding state data of the entire population of enzymes to a 3-state Markov chain model, where an enzyme can be folded, unfolded, or bleached, and the state that the enzyme occupies depends only on the previous state. The transition probability matrix is given by

$$TR = \begin{pmatrix} 1 - p_f - p_{off} & p_f & p_{off} \\ p_u & 1 - p_u - p_{off} & p_{off} \\ 0 & 0 & 1 \end{pmatrix} \qquad \text{(Equation S1)},$$

where p_f, p_u, and p_{off} are the probabilities that a molecule will fold, unfold or end by photobleaching, unbinding/desorption between two consecutive frames. The value of p_{off} is assumed identical for both folded and unfolded molecules. The values for p_f, p_u are estimated by maximizing the likelihood function,

$$LF(S|p_f, p_u) = \prod_k [\prod_{i=1} TR(S_{i-1,k}, S_{i,k}|p_f, p_u)] \quad \text{(Equation S2)},$$

where $\{S_{1,k} \cdots S_{n,k}\}$ is the sequence of observed folding states for the kth trajectory. The maximum likelihood estimate can be defined explicitly for this as

$$\hat{p}_u = \frac{N_{fu}(1-p_{off})}{N_{ff}+N_{fu}} \quad \text{(Equation S3)}$$

and

$$\hat{p}_f = \frac{N_{uf}(1-p_{off})}{N_{uu}+N_{uf}} \quad \text{(Equation S4)},$$

where N_{uf}, N_{uu}, N_{fu}, N_{ff}, and are the total number times an object folds, remains unfolded, unfolds, or remains folded, respectively, throughout the population. The mean binding and unbinding rate constants can be calculated as $k_f = -log\,(1 - \hat{p}_f/(1 - p_b))\,/\tau$ and $k_u = -log(1 - \hat{p}_u/(1 - p_b))/\tau$, respectively. Substituting Equation S3 and S4 into these equations simplifies to Equation 1, in the manuscript, which is independent of p_{off}.

Supporting Figures

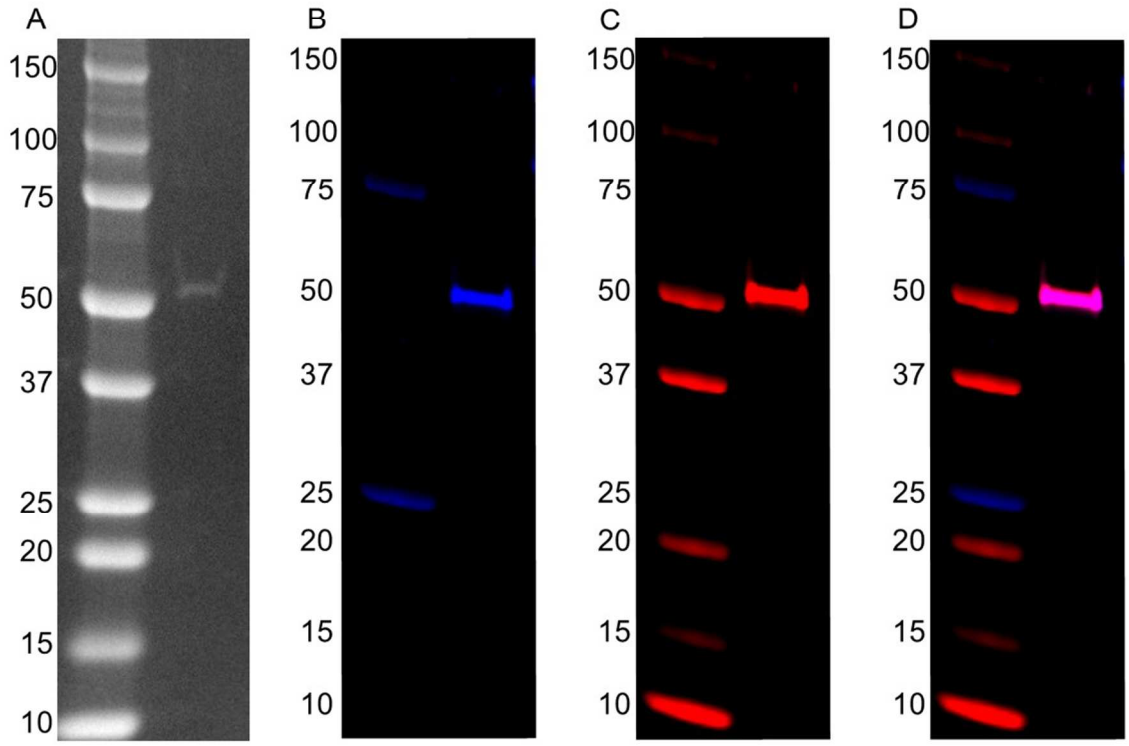

Figure S1. In-gel fluorescent imaging of NfsB site-specifically labeled with AF 488 and CF 633, which was used for SM-FRET studies. Upon SDS-PAGE, the band corresponding to site-specifically-labeled NfsB was stained with Coomassie (A) as well as imaged via direct excitation of AF 488 (B) or CF 633 (C). The overlay of images in panel B and C (D) confirm the covalent attachment of both AF488 and CF 633.

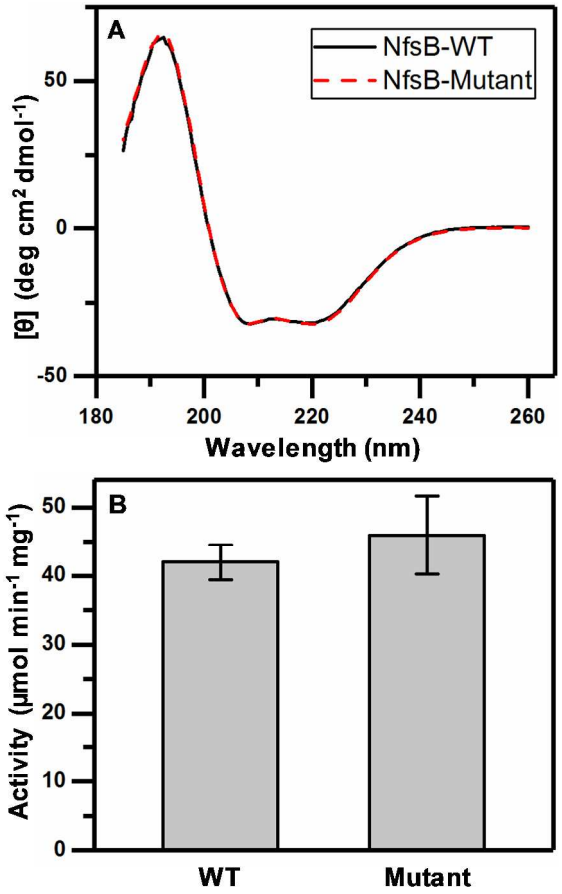

Figure S2. Characterization of the folding state and activity of the NfsB Ala89AzF/Ala315Cys double mutant. A) Circular dichroism spectrum of wild-type NfsB (solid black) and NfsB Ala89AzF/Ala315Cys (dash red), showing the structure of NfsB was unaffected by the mutations used for site-specific labeling. Each spectrum represents the average of three successive scans from 185-260 nm in 0.5 nm increments with an integration time of 0.5 s per increment. B) Specific activity of wild-type NfsB and NfsB Ala89AzF/Ala315Cys, showing the activity of NfsB was also unaffected by the mutations. Error bars represent standard deviation from three different experimental measurements.

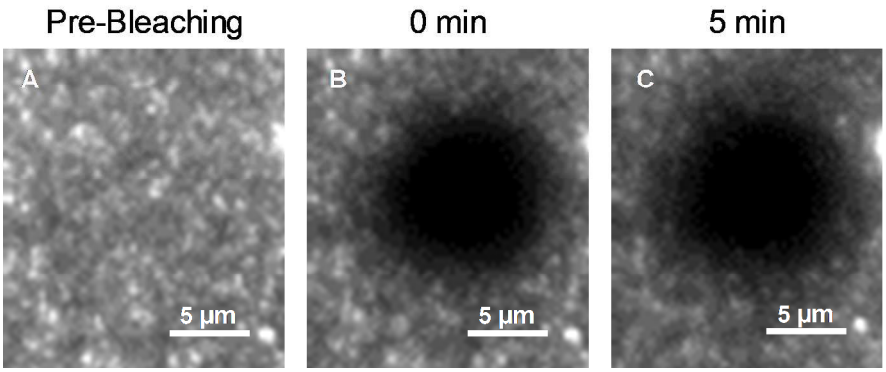

Figure S3. Fluorescent images of the 100% DOPG SLB containing 1% of the fluorescent lipid DOPE-LR before photo-bleaching (A), immediately after photo-bleaching (B), and 5 min after photo-bleaching (C). The fluorescence on the surface shows that lipid bilayers fused onto the glass wafers with high surface coverage, though continuous bilayers were not formed as demonstrated by the lack of recovery after photo-bleaching.

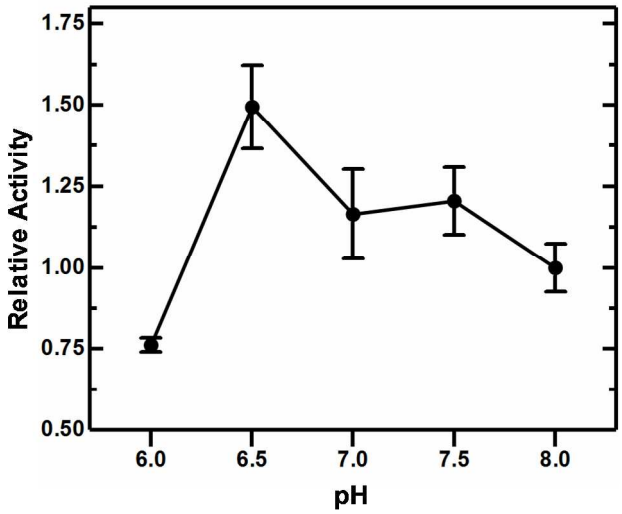

Figure S4. Relative specific activity of native NfsB in solution as a function of pH in 10 mM sodium phosphate normalized to activity in pH 8.0, which was the pH the buffer in SM experiments. The error bars represent the standard error of the specific activity of NfsB for four different NfsB concentrations.

Supporting Tables

Table S1. Mobile fraction (F_M) and diffusion coefficients (D_{FRAP}) for each SLB composition obtained from FRAP experiments. The values for F_M and D_{FRAP} for 75% and 100% DOPG SLBs could not be measured due to the lack of continuity in the bilayers. Uncertainties represent standard deviation of three replicate experiments.

SLB	F_M	D_{FRAP} ($\mu m^2/s$)
0 % DOPG	0.988 ± 0.005	1.2 ± 0.1
15 % DOPG	0.98 ± 0.02	0.8 ± 0.1
25 % DOPG	0.95 ± 0.04	0.8 ± 0.1
35 % DOPG	0.97 ± 0.04	0.74 ± 0.06
50 % DOPG	0.96 ± 0.04	0.81 ± 0.08

Table S2. Fitting parameters for D of DOPE-LR, folded NfsB, and unfolded NfsB as a function of DOPG. Uncertainties represent the standard deviation of the fits of 100 sub-samples obtained using a bootstrap method as described in the main paper.

Molecule	SLB	P_{fast}	D_{fast} ($\mu m^2/s$)	P_{slow}	D_{slow} ($\mu m^2/s$)
Lipid (DOPE-LR)	0 % DOPG	92.3 ± 0.3 %	3.92 ± 0.03	7.7 ± 0.3 %	0.182 ± 0.008
	15 % DOPG	90.0 ± 0.4 %	4.07 ± 0.01	10.0 ± 0.4 %	0.21 ± 0.02
	25 % DOPG	86.6 ± 0.5 %	4.17 ± 0.01	13.4 ± 0.5 %	0.38 ± 0.02
	35 % DOPG	84.2 ± 0.6 %	4.30 ± 0.04	15.8 ± 0.6 %	0.46 ± 0.02
	50 % DOPG	82.0 ± 0.5 %	4.41 ± 0.04	18.0 ± 0.5 %	0.49 ± 0.02
Folded NfsB	0 % DOPG	75 ± 2 %	3.6 ± 0.1	25 ± 2 %	0.21 ± 0.02
	15 % DOPG	86 ± 1 %	4.07 ± 0.08	14 ± 1 %	0.25 ± 0.04
	25 % DOPG	86.9 ± 0.5 %	3.65 ± 0.07	13.1 ± 0.5 %	0.25 ± 0.02
	35 % DOPG	87.0 ± 0.6 %	4.03 ± 0.05	13.0 ± 0.6 %	0.30 ± 0.03
	50 % DOPG	79 ± 1 %	4.2 ± 0.1	21 ± 1 %	0.27 ± 0.03
Unfolded NfsB	0 % DOPG	36 ± 5 %	3.0 ± 0.4	64 ± 5 %	0.17 ± 0.01
	15 % DOPG	41 ± 6 %	3.6 ± 0.4	59 ± 6 %	0.19 ± 0.05
	25 % DOPG	49 ± 7 %	3.5 ± 0.8	51 ± 7 %	0.22 ± 0.04
	35 % DOPG	57 ± 6 %	3.8 ± 0.6	43 ± 6 %	0.28 ± 0.09
	50 % DOPG	58 ± 5 %	3.7 ± 0.5	42 ± 5 %	0.26 ± 0.01

References

(1) Blumenthal, D.; Goldstien, L.; Edidin, M.; Gheber, L. A. Universal Approach to FRAP Analysis of Arbitrary Bleaching Patterns. *Sci. Rep.* **2015**, *5* (1), 11655.

(2) D. Axelrod, D.E. Koppel, J. Schelessinger, E. Elson, W. W. W. Mobility Measurement by Analysis of Fluorescence Photobeaching Recovery Kinetics. *Biophys. J.* **1976**, *16*, 1055–1069.

(3) Ziemba, B. P.; Falke, J. J. Lateral Diffusion of Peripheral Membrane Proteins on Supported Lipid Bilayers Is Controlled by the Additive Frictional Drags of (1) Bound Lipids and (2) Protein Domains Penetrating into the Bilayer Hydrocarbon Core. *Chem. Phys. Lipids* **2013**, *172–173*, 67–77.

(4) Knight, J. D.; Lerner, M. G.; Marcano-Velázquez, J. G.; Pastor, R. W.; Falke, J. J. Single Molecule Diffusion of Membrane-Bound Proteins: Window into Lipid Contacts and Bilayer Dynamics. *Biophys. J.* **2010**, *99* (9), 2879–2887.